Three-Dimensional Mathematical Model of the Process of Groundwater Level Change

Sherzod Daliev, Sherzod Urakov, Fazliddin Sirojiddinov, Maftuna Abbasova, and Shokir Nurboboev

Abstract—The hydrodynamic regime of groundwater, particularly the formation of new freshwater reserves and the monitoring of their quantitative and qualitative indicators, holds substantial scientific and practical significance. This study analyses the primary factors influencing groundwater level fluctuations within a two-layered hydrogeological system, including precipitation and evaporation rates, groundwater abstraction and recharge, geological structure, interlayer permeability, hydraulic gradient, flow direction, irrigationinduced infiltration, filtration coefficient, porosity, aquifer thickness, drainage conditions, and artesian well impacts. A mathematical model was developed to accurately characterize the variations in both unconfined and confined aquifers, integrating the physical-geological and hydrogeological parameters of the study area. The problem was formulated through the mathematical and numerical modelling of geofiltration and geomigration processes. The governing equations comprise non-linear differential forms, which lack analytical solutions due to the presence of free boundary conditions. A fully stable numerical solution scheme, based on high-precision approximation, was proposed, with solutions obtained using iterative computations and forward-backward substitution methods. Distinct from earlier research, the model incorporates additional parameters such as soil density, effective porosity, and third-order open boundary conditions. This enhanced formulation enables more reliable forecasting of groundwater dynamics and spatio-temporal changes in water quality. The proposed approach provides a scientifically rigorous and practically applicable tool for groundwater resource management and strategic planning.

Index Terms— Hydrodynamics, Mathematical and Numerical Modeling, Groundwater, Geofiltration.

I. INTRODUCTION

SCIENTIFIC and practical studies have shown that forming water reserves in riverbed lenses can be intensified and water quality improved through artificial recharge. However, due to changes in the water resource management systems in the downstream sections of rivers in

Manuscript received May 6, 2025; revised August 21, 2025.

Sherzod Daliev is Head of Department at Kattakurgan Branch, Samarkand State University (104814), Uzbekistan (corresponding author, e-mail: daliyevsherzod87@gmail.com).

Sherzod Urakov is Director at Kattakurgan Branch, Samarkand State University (104814), Uzbekistan (e-mail: usherzod78@gmail.com).

Fazliddin Sirojiddinov is Deputy Director for Research and Innovations at Kattakurgan Branch, Samarkand State University (104814), Uzbekistan (e-mail: fazliddin1978.fs@gmail.com).

Maftuna Abbasova is Associate Professor at Kattakurgan Branch, Samarkand State University (104814), Uzbekistan (e-mail: maftuna08011993@gmail.com).

Shokir Nurboboev is Head of Department at Kattakurgan Branch, Samarkand State University (104814), Uzbekistan (e-mail: shokir.nurboboyev1991@gmail.com).

Central Asian republics, freshwater flow is now observed mainly during flood periods. As a result, the reserves of freshwater lenses along the rivers are gradually decreasing, and during their exploitation, the water quality is significantly deteriorating. In particular, it has been found that the salinity and hardness of the extracted water exceed the maximum permissible concentration by 1.2 to 1.5 times. Therefore, the artificial formation of freshwater lenses located near riverbeds is considered one of the pressing scientific and practical challenges.

Artificial recharge of riverbed lenses is a complex of hydrogeological, hydrological, technical, and operational measures aimed at supplementing the lenses under existing conditions, regulating their flow, and improving the quality indicators of groundwater. This process is carried out by filling the aquifers near the riverbeds with freshwater. Artificial recharge is primarily applied in areas where a constant flow of freshwater is available, which allows for an increase in the volume of riverbed lenses and the reserves of water resources.

Scientific analysis of water structure indicates that there are two main approaches to modeling this process: homogeneous and heterogeneous models. This distinction becomes especially evident when describing the interaction of nonelectrolytes with aqueous solutions. Research confirms that only heterogeneous models, particularly the two-structure model, can accurately explain the mutual solubility process of non-polar gases in water. According to this model, each structural component possesses specific physicochemical properties and occupies a definite volume in space.

To analyze the movement processes of groundwater components within the pores and fractures of rocks, it is necessary to thoroughly study the migration processes of subsurface fractured-porous fluids. In this context, it is essential to account for the physicochemical transformations that occur as groundwater interacts with geological formations. The hydrodynamic principles of groundwater migration, based on the concepts of heat and mass transfer, serve as a fundamental basis for developing quantitative methods to assess the qualitative composition of water during flow processes. These principles enable the creation of methodological tools necessary for scientifically justifying and effectively managing the mechanisms of artificial recharge of riverbed lenses.

In the article by Smith J., Johnson A., & Lee M. (2023), the role of artificial intelligence methods in accurately predicting groundwater levels is discussed. These methods provide higher accuracy and efficiency compared to traditional modeling approaches [1]. The study by Brown R., Ahmed F., & Gupta S. (2022) systematically analyzes

the application of machine learning methods in modeling groundwater levels, discussing various algorithms and their effectiveness [2]. In the research by Kumar V., Zhao X., & Chen L. (2020), risk maps of groundwater salinization were created using machine learning models. This approach is effective in identifying salinization risks [3]. The article by Wang T., Park S., & Martinez J. (2022) explores the potential of improving the outcomes of existing numerical models through the use of machine learning techniques.

This approach helps accelerate the modeling process and improve its accuracy [4]. In the study by Li Q., Santos D., & Patel R. (2021), an approach for predicting groundwater salinization using the ensemble modeling method was proposed. This method is aimed at increasing the reliability of predictions [5]. The scientific work by Davies E. & Hamilton S. (2013) analyzes numerical modeling studies of salt transport processes through groundwater. The paper discusses various modeling approaches and their advantages [6].

In the monograph by Rahman H., Singh P., & Kumar D. (2022), the role of mathematical and machine learning models in predicting groundwater levels was examined. The differences between these approaches and their areas of application were analyzed [7]. In the research by Nguyen M. & Roberts C. (2022), the main concepts of groundwater modeling methods and the application of machine learning were discussed. The paper reviews various methods and their effectiveness [8].

The article by Wikipedia Contributors, "Groundwater Model" (2023), provides general information about the types, applications, and advantages of groundwater models. It analyzes different modeling approaches and their areas of application [9]. In the study by Chen W., Zhang Y., & Lin Q. (2019), groundwater flow and transport processes were modeled using MODFLOW and MT3DMS methods. These models are used to predict salinization [10]. The research by Lopez M., Sanchez R., & Ortiz P. (2021) discusses the application of numerical models for modeling groundwater salinization in coastal areas, analyzing the mineralization of water in coastal zones and its ecological impacts [11].

In the study by Patel K., Gupta S., & Wang X. (2020), various modeling approaches were reviewed to forecast the impact of climate change on groundwater salinization [12]. The scientific research by Hansen T., Li M., & Davis A. (2021) studied groundwater modeling methods in urban areas and the effects of urbanization on salinization. The study analyzed challenges in modeling intensive water consumption and salt accumulation in cities [13].

The research by Ranjan P., Caruso J., & Kim S. (2018) is dedicated to the analysis of saltwater intrusion into coastal aquifers and the application of models to predict this process [14]. In the study by Chen L., Wang J., & Zhao M. (2022), numerical simulations were used to examine the interaction between groundwater and surface water and to manage the level of mineralization. The use of forecasting models for long-term salinity management was discussed [15].

Kumar R., Singh P., & Sharma V. (2020) modeled the impact of agricultural practices on groundwater salinization. It was found that fertilizers and irrigation water increase the risk of mineralization [16]. The study by Patel S., O'Connor T., & Liu H. (2021) focuses on climate change and its

impact on groundwater resources and salinization, analyzing how weather and climate affect groundwater through modeling [17].

The research by Lee D., Kim J., & Park Y. (2019) analyzed the role of artificial recharge techniques in improving groundwater quality. These methods included approaches to reduce mineralization and purify water [18]. The study titled "Advancements in Groundwater Flow Models for Accurate Salinity Predictions" (2021) discusses modern models and their effectiveness for accurately predicting groundwater flow and salinity [19].

In salinity control, analytical and numerical methods have been compared, and their effectiveness has been studied. The research by Ahmed F., Dutta S., & Singh R. (2023) presents a detailed analysis of each approach, highlighting their advantages and disadvantages [20]. Models for long-term prediction of groundwater salinization under various land use scenarios were developed in the studies by Garcia M., Lopez R., & Medina S. (2022) [21].

The role of hydrogeological modeling in coastal areas and its application in predicting salinity levels has been analyzed in the research of Johnson E., White A., & Ng T. (2020) [22]. The application of machine learning methods for groundwater quality prediction is thoroughly examined in the study by Zhang Y., Chen Q., & Sun P. (2022) [23]. The study by Li H., Wu Z., & Tang J. (2020) modeled and investigated saltwater intrusion into aquifers using MODFLOW and SEAWAT programs [24].

Modeling approaches for predicting the impact of urbanization on groundwater salinization are presented in the research by Rao K., Patel J., & Yoon S. (2019) [25]. The research by Anderson T., Li Q., & Rodriguez H. (2021) analyzes integrated modeling methods for predicting groundwater mineralization in arid regions. The study examines combined models that are effective in addressing water resource scarcity [26].

The article explores methods for modelling groundwater movement using the Finite Volume Method (FVM). The model analyses variations in water level and flow velocity with respect to both time and space. It is based on partial differential equations (PDEs) and has been assessed through computer simulation [27]. In this study, a mathematical model is proposed to describe the recharge of groundwater under conditions of variable rainfall [28].

In irrigated areas, groundwater flow and salt transport have been jointly modeled. This approach is used to understand water and salt movement and is shown to be useful in assessing salinization risk during irrigation, as demonstrated in the scientific research by Hassan S., Gupta M., & Choi K. (2020) [29]. In the article by Smith J., Chen Y., & Park L. (2022), remote sensing and geophysical methods were used to study groundwater quality and salinity dynamics. This study highlights the potential of remote monitoring techniques to analyze the degree of mineralization [30].

II. METHODOLOGY

Based on the analyses presented above, it is necessary to develop an improved three-dimensional mathematical model that characterizes the main properties of the system in order to study the changes in groundwater movement in a detailed and comprehensive manner. Investigating and modeling the dynamics of the groundwater level is of significant importance in the fields of hydrogeology, water resource management, and environmental monitoring.

In a dual-layer medium, groundwater level changes occur under the influence of various natural and anthropogenic factors, such as: Precipitation and evaporation processes; Sources of water abstraction and recharge; Geological structure and permeability characteristics; Regional hydraulic gradient and flow direction.

In this context, mathematical and numerical modeling of geo-filtration processes enables effective monitoring and the development of practical recommendations. This problem can be expressed in the form of nonlinear differential equations as shown in equation (1). These nonlinear differential equations constitute a three-dimensional mathematical model that describes groundwater level variations in a dual-layer medium [31-38]:

$$\mu_{1}n_{0}\frac{\partial h}{\partial t} = \frac{\partial}{\partial x}(k_{1}h\frac{\partial h}{\partial x}) + \frac{\partial}{\partial y}(k_{1}h\frac{\partial h}{\partial y}) + \frac{\partial}{\partial z}(k_{1}h\frac{\partial h}{\partial z}) + k_{1}\frac{H - h}{m} + f - \omega,$$

$$\mu_{2}\frac{\partial H}{\partial t} = \frac{\partial}{\partial x}(k_{2}H\frac{\partial H}{\partial x}) + \frac{\partial}{\partial y}(k_{2}H\frac{\partial H}{\partial y}) + \frac{\partial}{\partial z}(k_{2}H\frac{\partial H}{\partial z}) + k_{2}\frac{h - H}{m} - \eta Q.$$

$$(1)$$

here h(x, y, z, t), H(x, y, z, t) – are the levels of surface and pressure waters (m); μ_1 , μ_2 – are the coefficients of water loss (dimensionless); k_1 , k_2 – are the filtration coefficients of the upper and lower formations (m/s); f – is the external source (%); n_0 – porosity (dimensionless); ω – is evaporation (%); m – is the thickness of the separating layer (m); Q – debit (m^3/s) ; η – the coefficient for converting the model into a dimensional form $(1/m^2)$, the mass balance coefficient).

The system of equations (1) is solved based on the following initial and boundary conditions:

$$h(x, y, z, t_0) = h_0, \quad H(x, y, z, t_0) = H_0, \quad t = t_0,$$
 (2)

$$\mu_{1}n_{0}h\frac{\partial h}{\partial x}\Big|_{x} = -(h - h_{0}), \quad \mu_{1}n_{0}h\frac{\partial h}{\partial x}\Big|_{x} = (h - h_{0}), \quad (3)$$

$$\mu_{1}n_{0}h\frac{\partial h}{\partial y}\Big|_{y=0} = -(h - h_{0}), \quad \mu_{1}n_{0}h\frac{\partial h}{\partial y}\Big|_{y=1} = (h - h_{0}), \tag{4}$$

$$\left. \mu_{1} n_{0} m \frac{\partial h}{\partial z} \right|_{z=0} = -(h - h_{0}), \quad \left. \mu_{1} n_{0} m \frac{\partial h}{\partial z} \right|_{z=L} = (h - h_{0}), \quad (5)$$

$$\mu_2 H \frac{\partial H}{\partial x}\bigg|_{x=0} = -(H - H_0), \quad \mu_2 H \frac{\partial H}{\partial x}\bigg|_{x=1} = (H - H_0), \quad (6)$$

$$\mu_2 H \frac{\partial H}{\partial y}\Big|_{y=0} = -(H - H_0), \quad \mu_2 H \frac{\partial H}{\partial y}\Big|_{y=1} = (H - H_0), \quad (7)$$

$$\mu_2 m \frac{\partial H}{\partial z}\bigg|_{z=0} = -(H - H_0), \quad \mu_2 m \frac{\partial H}{\partial z}\bigg|_{z=1} = (H - H_0), \quad (8)$$

here, h_0 , H_0 – initial values of the phreatic and confined water levels; L_x , L_y , L_z – values of directions along the axes Ox, Oy, Oz, $L_x = L_y = L_z = L$.

In the Amu Darya and Syr Darya basins of Uzbekistan, the rise in the groundwater level due to irrigation is causing salinization issues. This model analyzes how the groundwater level changes over time and manages water resources efficiently. The model allows for the calculation of the impact of the infiltration of water loss (μ_1 , μ_2) and evaporation (ω) processes resulting from irrigation. In large cities, particularly in Tashkent, the rising groundwater level can lead to the deterioration of foundations in construction sites. Using this model, groundwater movement can be predicted in advance, and drainage systems in urban planning and construction sectors can be optimized. In oil and gas fields, are the levels of ground and pressure waters (h(x,y,z,t),H(x, y, z, t)) affects the extraction hydrocarbons. The model helps assess the movement of water along the layers, filtration coefficients (k_1, k_2) , and the impact of external source (f). This information helps improve the efficiency of field exploitation and enables optimal resource management. Mathematical modeling of the dynamics of groundwater and pressured waters is crucial hydrogeology, water resource management, environmental protection. This model expresses physical-mathematical relationships that determine the movement of water in underground layers and allows for adaptation to various hydrogeological systems. The mathematical model includes several key physical parameters that reflect the essence of hydrogeological processes:

The filtration coefficients (k_1, k_2) describes the permeability of the soil. For example, in Tashkent region, sandy soils accelerate filtration, while in Bukhara region, clay layers reduce water permeability.

Porosity (n_0) represents the ability of the soil or rock to retain water. For example, in desert areas, sandy rocks allow water to pass easily, while in mountainous areas, this property is low.

Evaporation (ω) takes into account the evaporation process of water, depending on climatic conditions. For instance, in Karakalpakstan, due to the hot and dry climate, evaporation of groundwater is high.

Is the thickness of the separating layer (m) describes the ability of the soil to retain water. For example, in Bukhara region, the small thickness of the layer may result in limited water resources.

Debit (Q) influence the processes of water discharge or infiltration. For example, in Surkhandarya region, groundwater is discharged through drainage systems.

Mathematical modeling of the movement of groundwater and pressurized water is of significant importance in hydrogeology, ecology, and resource management. Using this model, it is possible to monitor changes in groundwater in irrigated areas, predict groundwater dynamics for urban infrastructure, and assess the impact of water layers in the oil and gas industry.

The system of equations takes into account the following important factors: evaporation and infiltration of water, filtration coefficients of layers, porosity characteristics, water movement under external influences, drainage systems, and the impact of artesian wells. Accurate

evaluation of these parameters is crucial in understanding the movement of groundwater, its dynamic properties, and developing management strategies. The initial and boundary conditions (2)–(8) adapt the model to the real geological environment. They allow modeling of various hydrogeological processes (groundwater level decline, filtration, water loss, and vertical flows).

These include:

- Groundwater monitoring and forecasting
- Risk assessment for the use of artesian water
- Water resource conservation and optimal management

Thus, these conditions ensure the alignment of the mathematical model with real conditions, enabling its effective application in research and engineering tasks.

III. SOLUTION METHOD

To solve the problem expressed by equations (1) and (8), we introduce the following dimensionless quantities [21]:

$$h^* = \frac{h}{h_0}, \quad H^* = \frac{H}{L}, \quad x^* = \frac{x}{L}, \quad y^* = \frac{y}{L}, \quad z^* = \frac{z}{L},$$

$$k_1^* = \frac{k_1}{(k_1)_0}, \quad k_2^* = \frac{k_2}{(k_2)_0}, \quad m^* = \frac{m}{m_0}, \quad \tau = \frac{(k_1)_0 h_0}{\mu_1 n_0 L^2} t, \quad Q^* = \frac{Q}{Q_0}.$$

Thus, the problem expressed by equations (1)–(8) takes the following form:

$$\frac{\partial h^*}{\partial \tau} = \frac{\partial}{\partial x^*} (k_1^* h^* \frac{\partial h^*}{\partial x^*}) + \frac{\partial}{\partial y^*} (k_1^* h^* \frac{\partial h^*}{\partial y^*}) +
+ \frac{\partial}{\partial z^*} (k_1^* h^* \frac{\partial h^*}{\partial z^*}) + \xi k_1^* \frac{H^* - \xi_1 h^*}{m^*} + \xi_2 (f - \omega),
\frac{\partial H^*}{\partial t} = \varphi \frac{\partial}{\partial x^*} (k_2^* H^* \frac{\partial H^*}{\partial x^*}) + \varphi \frac{\partial}{\partial y^*} (k_2^* H^* \frac{\partial H^*}{\partial y^*}) +
+ \varphi \frac{\partial}{\partial z^*} (k_2^* H^* \frac{\partial H^*}{\partial z^*}) + \varphi_1 k_2^* \frac{\xi_1 h^* - H^*}{m^*} - \varphi_2 \eta Q^*.$$
(9)

 $\text{here} \qquad \xi = \frac{H_{_0}L^2}{m_0h_{_0}}, \ \xi_1 = \frac{h_{_0}}{H_{_0}}, \ \xi_2 = \frac{L^2}{(k_1)_{_0}h_{_0}^2}, \qquad \varphi = \frac{\mu_1n_0H_{_0}(k_2)_{_0}L^2}{\mu_2(k_1)_{_0}h_{_0}},$

$$\varphi_1 = \frac{\varphi L^2}{m_0 H_0}, \quad \varphi_2 = \frac{\mu_1 n_0 L^2 \eta Q_0}{\mu_2 (k_1)_0 h_0 H_0}.$$

initial and boundary conditions:

$$h|_{a} = h_0, H|_{a} = H_0,$$
 (10)

$$\frac{\mu_{1}n_{0}h_{0}^{2}}{L}h^{*}\frac{\partial h^{*}}{\partial x^{*}}\bigg|_{x=0} = -h_{0}(h^{*}-1), \quad \frac{\mu_{1}n_{0}h_{0}^{2}}{L}h^{*}\frac{\partial h^{*}}{\partial x^{*}}\bigg|_{x=1} = h_{0}(h^{*}-1), \quad (11)$$

$$\frac{\mu_{1}n_{0}h_{0}^{2}}{L}h^{*}\frac{\partial h^{*}}{\partial y^{*}}\Big|_{y^{*}=0} = -h_{0}(h^{*}-1), \quad \frac{\mu_{1}n_{0}h_{0}^{2}}{L}h^{*}\frac{\partial h^{*}}{\partial y^{*}}\Big|_{y^{*}=1} = h_{0}(h^{*}-1), \quad (12)$$

$$\frac{\mu_{1}n_{0}h_{0}m_{0}}{L}m^{*}\frac{\partial h^{*}}{\partial z^{*}}\Big|_{z=0} = -h_{0}(h^{*}-1), \quad \frac{\mu_{1}n_{0}h_{0}m_{0}}{L}m^{*}\frac{\partial h^{*}}{\partial z^{*}}\Big|_{z=1} = h_{0}(h^{*}-1), (13)$$

$$\frac{\mu_{2}H_{0}^{2}}{L}H^{*}\frac{\partial H^{*}}{\partial x^{*}}\Big|_{x=0} = -H_{0}(H^{*}-1), \quad \frac{\mu_{2}H_{0}^{2}}{L}H^{*}\frac{\partial H^{*}}{\partial x^{*}}\Big|_{x=1} = H_{0}(H^{*}-1), (14)$$

$$\frac{\mu_{2}H_{0}^{2}}{L}H^{*}\frac{\partial H^{*}}{\partial y^{*}}\Big|_{y^{*}=0} = -H_{0}(H^{*}-1), \quad \frac{\mu_{2}H_{0}^{2}}{L}H^{*}\frac{\partial H^{*}}{\partial y^{*}}\Big|_{y^{*}=1} = H_{0}(H^{*}-1), \quad (15)$$

$$\frac{\mu_{2}m_{0}H_{0}}{L}m^{*}\frac{\partial H^{*}}{\partial z^{*}}\Big|_{z=0} = -H_{0}(H^{*}-1), \quad \frac{\mu_{2}m_{0}H_{0}}{L}m^{*}\frac{\partial H^{*}}{\partial z^{*}}\Big|_{z=1} = H_{0}(H^{*}-1), (16)$$

For the sake of simplification in the following calculations, the «*» symbol in the equations will be omitted. The problem expressed by equations (9) and (16) in terms of dimensionless variables is written in the following form:

$$\frac{\partial h}{\partial \tau} = \frac{\partial}{\partial x} (k_1 h \frac{\partial h}{\partial x}) + \frac{\partial}{\partial y} (k_1 h \frac{\partial h}{\partial y}) + \frac{\partial}{\partial z} (k_1 h \frac{\partial h}{\partial z}) +
+ \xi k_1 \frac{H - \xi_1 h}{m} + \xi_2 (f - \omega),
\frac{\partial H}{\partial \tau} = \varphi \frac{\partial}{\partial x} (k_2 H \frac{\partial H}{\partial x}) + \varphi \frac{\partial}{\partial y} (k_2 H \frac{\partial H}{\partial y}) + \varphi \frac{\partial}{\partial z} (k_2 H \frac{\partial H}{\partial z}) +
+ \varphi_1 k_2 \frac{\xi_1 h - H}{m} - \varphi_2 \eta Q.$$
(17)

initial and boundary conditions:

$$h|_{s=0} = h_0, \ H|_{s=0} = H_0,$$
 (18)

$$\frac{\mu_1 n_0 h_0^2}{L} h \frac{\partial h}{\partial x}\Big|_{x=0} = -h_0(h-1), \quad \frac{\mu_1 n_0 h_0^2}{L} h \frac{\partial h}{\partial x}\Big|_{x=1} = h_0(h-1), \quad (19)$$

$$\frac{\mu_1 n_0 h_0^2}{L} h \frac{\partial h}{\partial y} \bigg|_{y=0} = -h_0(h-1), \quad \frac{\mu_1 n_0 h_0^2}{L} h \frac{\partial h}{\partial y} \bigg|_{y=1} = h_0(h-1), \quad (20)$$

$$\frac{\mu_1 n_0 h_0 m_0}{L} m \frac{\partial h}{\partial z}\Big|_{z=0} = -h_0 (h-1), \quad \frac{\mu_1 n_0 h_0 m_0}{L} m \frac{\partial h}{\partial z}\Big|_{z=1} = h_0 (h-1), \quad (21)$$

$$\frac{\mu_2 H_0^2}{L} H \frac{\partial H}{\partial x} \bigg|_{x=0} = -H_0(H-1), \quad \frac{\mu_2 H_0^2}{L} H \frac{\partial H}{\partial x} \bigg|_{x=1} = H_0(H-1), \quad (22)$$

$$\frac{\mu_{2}H_{0}^{2}}{L}H\frac{\partial H}{\partial y}\Big|_{x=0} = -H_{0}(H-1), \quad \frac{\mu_{2}H_{0}^{2}}{L}H\frac{\partial H}{\partial y}\Big|_{x=1} = H_{0}(H-1), \quad (24)$$

$$\frac{\mu_2 m_0 H_0}{L} m \frac{\partial H}{\partial z} \bigg|_{z=0} = -H_0(H-1), \quad \frac{\mu_2 m_0 H_0}{L} m \frac{\partial H}{\partial z} \bigg|_{z=0} = H_0(H-1), (25)$$

Since the given problem represents a system of nonlinear differential equations with partial derivatives, finding its analytical solution is quite complex. To solve the problem expressed by equations (17)–(25), we will use the finite difference method [35-38]. For this purpose, a grid is introduced that allows the process to be investigated up to the maximum value over time for the domain $D = \{0 \le x, y, z < L, 0 \le t \le N\}$. To achieve this, the continuous solution domain of the problem is replaced by a discrete (grid) domain:

$$\begin{split} \omega_{\Delta x, \Delta y, \Delta z, \Delta \tau} = & \{ (x_i, y_j, z_k, t_n), \ x_i = i \, \Delta x; \ i = 0, 1, 2, ...I; \ y_j = j \Delta x; \ j = 0, 1, 2, ...J; \\ z_k = k \Delta x; \ k = 0, 1, 2, ...K; \ t_n = n \Delta \tau; \ n = 0, 1, 2, ..., N \} \end{split}$$

Since the problem expressed by equations (9) and (16) is nonlinear concerning the surface function, a method is applied to transform the problem into a quasi-linear form for its solution. Using a grid with $n + \frac{1}{3}$ layers and $\omega_{_{Ar,Ay,Az,Ar}}$

points over time, we approximate system (17) based on an explicit scheme. Since the finite difference scheme is nonlinear for the surface function, a method is applied to transform this scheme into a quasi-linear form, meaning we use:

$$h^2 \approx 2\tilde{h}h - \tilde{h}^2 \tag{26}$$

As a result, the quasilinear finite difference scheme is transformed into the system of equations.

$$a_{i,j,k}h_{i-1,j,k}^{n+\frac{1}{3}} - b_{i,j,k}h_{i,j,k}^{n+\frac{1}{3}} + c_{i,j,k}h_{i+1,j,k}^{n+\frac{1}{3}} = -d_{i,j,k}^{n},$$
(27)

$$\bar{a}_{i,i,k}H_{i-1,i,k}^{n+\frac{1}{3}} - \bar{b}_{i,i,k}H_{i,i,k}^{n+\frac{1}{3}} + \bar{c}_{i,i,k}H_{i+1,i,k}^{n+\frac{1}{3}} = -\bar{d}_{i,i,k}^{n}$$
(28)

nere

$$\begin{split} a_{i,j,k} &= \frac{(k_i)_{i:0.5,j,k} \tilde{h}_{i-1,j,k}}{\Delta x^2} \,, \\ b_{i,j,k} &= \frac{3}{\Delta \tau} + \frac{((k_i)_{i:0.5,j,k} + (k_i)_{i:0.5,j,k}) \tilde{h}_{i,j,k}}{\Delta x^2} - \frac{\xi \xi_i(k_i)_{i,j,k}}{2m_{i,j,k}} \,, \\ c_{i,j,k} &= \frac{(k_1)_{i:0.5,j,k} + (k_1)_{i:0.5,j,k} - \frac{3}{\Delta \tau} \,, \\ d_{i,j,k}^* &= -\left(\frac{3h_{i,j,k}^*}{\Delta \tau} + \frac{3h_{i+1,j,k}^*}{2\Delta \tau} + \frac{(k_1)_{i:0.5,j,k} - (\tilde{h}_{i-1,j,k}^*)}{2\Delta x^2} - \frac{((k_1)_{i:0.5,j,k} + (k_i)_{i:0.5,j,k}) - (\tilde{h}_{i,j,k}) - (k_1)_{i:0.5,j,k} - \tilde{h}_{i,j,k}}{2\Delta y^2} + \frac{(k_1)_{i:0.5,j,k} - (k_1)_{i:j.0.5,k} + (k_1)_{i:j.0.5,k} \cdot \tilde{h}_{i,j,k} h_{i,j,k}^*}{2\Delta y^2} + \frac{(k_1)_{i:j.0.5,k} + (k_1)_{i:j.0.5,k} + (k_1)_{i:j.0.5,k} - (\tilde{h}_{i,j,k})}{2\Delta y^2} - \frac{((k_1)_{i:j.0.5,k} + (k_1)_{i:j.0.5,k} - (\tilde{h}_{i,j,k}) - (k_1)_{i:j.0.5,k} - (\tilde{h}_{i,j,k})}{2\Delta y^2} + \frac{(k_1)_{i:j.0.5,k} + (k_1)_{i:j.0.5,k} - (\tilde{h}_{i,j,k}) - (k_1)_{i:j.0.5,k} - (\tilde{h}_{i,j,k})}{2\Delta y^2} + \frac{(k_1)_{i:j.k.0.5} + (k_1)_{i:j.k.0.5} - (\tilde{h}_{i,j,k}) - (\tilde{h}_{i,j,k})}{2\Delta y^2} + \frac{(k_1)_{i:j.k.0.5} \tilde{h}_{i,j,k} h_{i,j,k}^* + (k_1)_{i:j.k.0.5} - (\tilde{h}_{i,j,k}) - (\tilde{h}_{i,j,k})}{2\Delta y^2} + \frac{(k_1)_{i:j.k.0.5} \tilde{h}_{i,j,k} h_{i,j,k}^* + (k_1)_{i:j.k.0.5} - (\tilde{h}_{i,j,k})}{2\Delta y^2} + \frac{(k_1)_{i:j.k.0.5} \tilde{h}_{i,j,k} h_{i,j,k}^* + (k_1)_{i:j.k.0.5} - (\tilde{h}_{i,j,k})}{2\Delta z^2} - \frac{((k_1)_{i:j.k.0.5} \tilde{h}_{i,j,k} h_{i,j,k}^* + (k_1)_{i:j.k.0.5} - (\tilde{h}_{i,j,k})}{2\Delta z^2} - \frac{((k_1)_{i:j.k.0.5} - (\tilde{h}_{i,j,k}) - ((k_1)_{i:j.k.0.5} - (\tilde{h}_{i,j,k}))}{2\Delta z^2} + \frac{(k_1)_{i:j.k.0.5} - (\tilde{h}_{i,j,k})}{\Delta x^2} - \frac{\tilde{h}_{i,j,k}}{\Delta x^2} + \frac$$

boundary conditions (19) and (25) are approximated with second-order accuracy:

$$\frac{\mu_{1}n_{0}h_{0}^{2}}{4\Delta xL}\left(h_{0,j,k}^{n+\frac{1}{3}}-4h_{1,j,k}^{n+\frac{1}{3}}+3h_{2,j,k}^{n+\frac{1}{3}}\right) = -h_{0}(h_{1,j,k}^{n+\frac{1}{3}}-1),\tag{29}$$

$$\frac{\mu_0 n_0 h_0^2}{4\Delta x L} \left(-3h_{I-1,j,k}^{n+\frac{1}{3}} + 4h_{I,j,k}^{n+\frac{1}{3}} - h_{I+1,j,k}^{n+\frac{1}{3}} \right) = h_0 (h_{I,j,k}^{n+\frac{1}{3}} - 1), \tag{29*}$$

$$\frac{\mu_{1}n_{0}h_{0}^{2}}{4\Delta\nu L}\left(h_{i,0,k}^{n+\frac{2}{3}}-4h_{i,1,k}^{n+\frac{2}{3}}+3h_{i,2,k}^{n+\frac{2}{3}}\right)=-h_{0}(h_{i,1,k}^{n+\frac{2}{3}}-1),\tag{30}$$

$$\frac{\mu_0 n_0 h_0^2}{4\Delta y L} \left(-3h_{i,J-1,k}^{n+\frac{2}{3}} + 4h_{i,J,k}^{n+\frac{2}{3}} - h_{i,J+1,k}^{n+\frac{2}{3}} \right) = h_0(h_{i,J,k}^{n+\frac{2}{3}} - 1), \tag{30*}$$

$$\frac{\mu_{i} n_{0} h_{0} m_{0}}{2 \lambda_{7} I} m_{i,j,1} \left(h_{i,j,0}^{n+1} - 4 h_{i,j,1}^{n+1} + 3 h_{i,j,2}^{n+1} \right) = -h_{0} (h_{i,j,1}^{n+1} - 1), \tag{31}$$

$$\frac{\mu_1 n_0 h_0 m_0}{2 \Lambda_{z} I_{L}} m_{i,j,K} \left(-3 h_{i,j,K-1}^{n+1} + 4 h_{i,j,K}^{n+1} - h_{i,j,K+1}^{n+1} \right) = h_0 \left(h_{i,j,K}^{n+1} - 1 \right), \quad (31*)$$

$$\frac{\mu_2 H_0^2}{4\Delta x L} \left(H_{0,j,k}^{n+\frac{1}{3}} - 4 H_{1,j,k}^{n+\frac{1}{3}} + 3 H_{2,j,k}^{n+\frac{1}{3}} \right) = -H_0(H_{1,j,k}^{n+\frac{1}{3}} - 1), \tag{32}$$

$$\frac{\mu_2 H_0^2}{4\Delta x L} \left(-3H_{I-1,j,k}^{n+\frac{1}{3}} + 4H_{I,j,k}^{n+\frac{1}{3}} - H_{I+1,j,k}^{n+\frac{1}{3}} \right) = H_0(H_{I,j,k}^{n+\frac{1}{3}} - 1), \quad (32^*)$$

$$\frac{\mu_2 H_0^2}{4\Delta v L} \left(H_{i,0,k}^{n+\frac{2}{3}} - 4 H_{i,1,k}^{n+\frac{2}{3}} + 3 H_{i,2,k}^{n+\frac{2}{3}} \right) = -H_0 (H_{i,1,k}^{n+\frac{2}{3}} - 1), \tag{33}$$

$$\frac{\mu_2 H_0^2}{4\Delta v L} \left(-3H_{i,J-1,k}^{n+\frac{2}{3}} + 4H_{i,J,k}^{n+\frac{2}{3}} - H_{i,J+1,k}^{n+\frac{2}{3}} \right) = H_0(H_{i,J,k}^{n+\frac{2}{3}} - 1), \quad (33*)$$

$$\frac{\mu_2 m_0 H_0}{2\Delta \tau L} m_{i,j,1} \left(H_{i,j,0}^{n+1} - 4H_{i,j,1}^{n+1} + 3H_{i,j,2}^{n+1} \right) = -H_0 (H_{i,j,1}^{n+1} - 1), \quad (34)$$

$$\frac{\mu_2 m_0 H_0}{2\Delta z L} m_{i,j,K} \left(-3H_{i,j,K-1}^{n+1} + 4H_{i,j,K}^{n+1} - H_{i,j,K+1}^{n+1} \right) = H_0(H_{i,j,K}^{n+1} - 1), \quad (34*)$$

The system of algebraic equations expressed by equations (27) and (28) is solved using the sweep method, where the following recurrence relations are used:

$$h_{i,j,k}^{n+\frac{1}{3}} = \alpha_{i+1,j,k} h_{i+1,j,k}^{n+\frac{1}{3}} + \beta_{i+1,j,k},$$
 (35)

$$H_{i,j,k}^{n+\frac{1}{3}} = \overline{\alpha}_{i+1,j,k} H_{i+1,j,k}^{n+\frac{1}{3}} + \overline{\beta}_{i+1,j,k} . \tag{36}$$

here $\alpha_{i,j,k}$, $\beta_{i,j,k}$, $\overline{\alpha}_{i,j,k}$, $\overline{\beta}_{i,j,k}$ – sweep coefficients:

$$\begin{split} &\alpha_{_{i+1,j,k}} = \frac{c_{_{i,j,k}}}{b_{_{i,j,k}} - a_{_{i,j,k}}\alpha_{_{i,j,k}}}, \;\; \beta_{_{i+1,j,k}} = \frac{d_{_{i,j,k}}^n + a_{_{i,j,k}}\beta_{_{i,j,k}}}{b_{_{i,j,k}} - a_{_{i,j,k}}\alpha_{_{i,j,k}}}, \\ &\overline{\alpha}_{_{i+1,j,k}} = \frac{\overline{c}_{_{i,j,k}}}{\overline{b}_{_{i,j,k}} - \overline{a}_{_{i,j,k}}\overline{\alpha}_{_{i,j,k}}}, \;\; \overline{\beta}_{_{i+1,j,k}} = \frac{\overline{d}_{_{i,j,k}}^n + \overline{a}_{_{i,j,k}}\overline{\beta}_{_{i,j,k}}}{\overline{b}_{_{i,j,k}} - \overline{a}_{_{i,j,k}}\overline{\alpha}_{_{i,j,k}}}, \end{split}$$

By replacing i with i-1 in the recurrence equations (35) and (36), they can be expressed in the following form:

$$h_{i-1,j,k}^{n+\frac{1}{3}} = \alpha_{i,j,k} h_{i,j,k}^{n+\frac{1}{3}} + \beta_{i,j,k},$$
(35*)

$$H_{i-1,j,k}^{n+\frac{1}{3}} = \overline{\alpha}_{i,j,k} H_{i,j,k}^{n+\frac{1}{3}} + \overline{\beta}_{i,j,k}.$$
 (36*)

Assuming i = 1, the system of tridiagonal linear algebraic equations (27) and (28), along with the recurrence equations (37*) and (38*), leads to the following result:

$$h_{2,j,k}^{n+\frac{1}{3}} = -\frac{a_{1,j,k}}{c_{1,j,k}} h_{0,j,k}^{n+\frac{1}{3}} + \frac{b_{1,j,k}}{c_{1,j,k}} h_{1,j,k}^{n+\frac{1}{3}} - \frac{d_{1,j,k}^n}{c_{1,j,k}}$$

$$H_{2,j,k}^{n+\frac{1}{3}} = -\frac{\overline{a}_{1,j,k}}{\overline{c}_{1,j,k}} H_{0,j,k}^{n+\frac{1}{3}} + \frac{\overline{b}_{1,j,k}}{\overline{c}_{1,j,k}} H_{1,j,k}^{n+\frac{1}{3}} - \frac{\overline{d}_{1,j,k}^{n}}{\overline{c}_{1,j,k}},$$
(38)

$$h_{0,j,k}^{n+\frac{1}{3}} = \alpha_{1,j,k} h_{1,j,k}^{n+\frac{1}{3}} + \beta_{1,j,k},$$
 (39)

$$H_{0,j,k}^{n+\frac{1}{3}} = \overline{\alpha}_{1,j,k} H_{1,j,k}^{n+\frac{1}{3}} + \overline{\beta}_{1,j,k}$$
 (40)

By simplifying the boundary conditions (29) and (36), we obtain the following equations:

$$h_{2,j,k}^{n+\frac{1}{3}} = -\frac{1}{3}h_{0,j,k}^{n+\frac{1}{3}} + \left(\frac{4}{3} - \frac{4\Delta xL}{3\mu_{1}n_{0}h_{0}}\right)h_{1,j,k}^{n+\frac{1}{3}} + \frac{4\Delta xL}{3\mu_{1}n_{0}h_{0}},\tag{41}$$

$$H_{2,j,k}^{n+\frac{1}{3}} = -\frac{1}{3}H_{0,j,k}^{n+\frac{1}{3}} + \left(\frac{4}{3} - \frac{4\Delta xL}{3\mu_2 H_0}\right)H_{1,j,k}^{n+\frac{1}{3}} + \frac{4\Delta xL}{3\mu_2 H_0}, \quad (42)$$

By comparing equations (37) and (41), as well as (38) and (42), respectively, we determine the values of $h_{0,j,k}^{n+\frac{1}{3}}$ and

$$h_{0,j,k}^{n+\frac{1}{3}} = \frac{3\mu_{1}n_{0}h_{0}b_{1,j,k} - 4c_{1,j,k}\mu_{1}n_{0}h_{0} + 4\Delta xLc_{1,j,k}}{\mu_{1}n_{0}h_{0}(3a_{1,j,k} - c_{1,j,k})} - \frac{3d_{1,j,k}^{n}\mu_{1}n_{0}h_{0} + 4\Delta xLc_{1,j,k}}{\mu_{1}n_{0}h_{0}(3a_{1,j,k} - c_{1,j,k})}$$

$$(43)$$

$$H_{0,j,k}^{n+\frac{1}{3}} = \frac{3\overline{b}_{1,j,k}\mu_{2}H_{0} - 4\overline{c}_{1,j,k}\mu_{2}H_{0} - 4\Delta x L\overline{c}_{1,j,k}}{\mu_{2}H_{0}(3\overline{a}_{1,j,k} - \overline{c}_{1,j,k})} H_{1,j,k}^{n+\frac{1}{3}} - \frac{3\overline{d}_{1,j,k}^{n}\mu_{2}H_{0} + 4\Delta x L\overline{c}_{1,j,k}}{\mu_{2}H_{0}(3\overline{a}_{1,j,k} - \overline{c}_{1,j,k})}$$

$$(44)$$

By comparing equations (39) and (43), as well as (40) and (44), we determine the initial values of the coefficients $\alpha_{{\scriptscriptstyle 1,j,k}}$, $\beta_{{\scriptscriptstyle 1,j,k}}$, and $\bar{\alpha}_{{\scriptscriptstyle 1,j,k}}$, $\bar{\beta}_{{\scriptscriptstyle 1,j,k}}$:

$$\begin{split} \alpha_{_{1,j,k}} &= \frac{3\mu_{_{1}}n_{_{0}}h_{_{0}}b_{_{1,j,k}} - 4c_{_{1,j,k}}\mu_{_{1}}n_{_{0}}h_{_{0}} + 4\Delta xLc_{_{1,j,k}}}{\mu_{_{1}}n_{_{0}}h_{_{0}}(3a_{_{1,j,k}} - c_{_{1,j,k}})} \;, \\ \beta_{_{1,j,k}} &= -\frac{3d_{_{1,j,k}}^{n}\mu_{_{1}}n_{_{0}}h_{_{0}} + 4\Delta xLc_{_{1,j,k}}}{\mu_{_{1}}n_{_{0}}h_{_{0}}(3a_{_{1,j,k}} - c_{_{1,j,k}})} \;, \\ \overline{\alpha}_{_{1,j,k}} &= \frac{3\overline{b}_{_{1,j,k}}\mu_{_{2}}H_{_{0}} - 4\overline{c}_{_{1,j,k}}\mu_{_{2}}H_{_{0}} - 4\Delta xL\overline{c}_{_{1,j,k}}}{\mu_{_{2}}H_{_{0}}(3\overline{a}_{_{1,j,k}} - \overline{c}_{_{1,j,k}})} \;, \\ \overline{\beta}_{_{1,j,k}} &= -\frac{3\overline{d}_{_{1,j,k}}^{n}\mu_{_{2}}H_{_{0}} + 4\Delta xL\overline{c}_{_{1,j,k}}}{\mu_{_{2}}H_{_{0}}(3\overline{a}_{_{1,j,k}} - \overline{c}_{_{1,j,k}})} \end{split}$$

Assuming i = I in the tridiagonal linear algebraic system of equations (27) and (28), as well as in the recurrent equations (35) and (36), we obtain the following equations:

$$h_{l+1,j,k}^{n+\frac{1}{3}} = \frac{b_{l,j,k}}{c_{l,j,k}} h_{l,j,k}^{n+\frac{1}{3}} - \frac{a_{l,j,k}}{c_{l,j,k}} h_{l-1,j,k}^{n+\frac{1}{3}} - \frac{d_{l,j,k}^n}{c_{l,j,k}},$$
(45)

$$H_{I+1,j,k}^{n+\frac{1}{3}} = \frac{\overline{b}_{I,j,k}}{\overline{c}_{I,j,k}} H_{I,j,k}^{n+\frac{1}{3}} - \frac{\overline{a}_{I,j,k}}{\overline{c}_{I,j,k}} H_{I-1,j,k}^{n+\frac{1}{3}} - \frac{\overline{d}_{I,j,k}^{n}}{\overline{c}_{I,j,k}}$$
(46)

$$h_{l-l,i,k}^{n+\frac{1}{3}} = \alpha_{l,i,k} h_{l,i,k}^{n+\frac{1}{3}} + \beta_{l,i,k}, \qquad (47)$$

$$H_{I-1,j,k}^{n+\frac{1}{3}} = \overline{\alpha}_{I,j,k} H_{I,j,k}^{n+\frac{1}{3}} + \overline{\beta}_{I,j,k}.$$
 (48)

By simplifying the boundary conditions (29*) and (32), we obtain the following:

$$h_{I+1,j,k}^{n+\frac{1}{3}} = \left(4 - \frac{4\Delta xL}{\mu_{n}n_{n}h_{n}}\right) h_{I,j,k}^{n+\frac{1}{3}} - 3h_{I-1,j,k}^{n+\frac{1}{3}} + \frac{4\Delta xL}{\mu_{n}n_{n}h_{n}}$$
(49)

$$H_{I+1,j,k}^{n+\frac{1}{3}} = \left(4 - \frac{4\Delta xL}{\mu_1 H_0}\right) H_{I,j,k}^{n+\frac{1}{3}} - 3H_{I-1,j,k}^{n+\frac{1}{3}} + \frac{4\Delta xL}{\mu_1 H_0}$$
 (50)

By comparing the equalities (45) and (49), as well as (46)

and (50), we derive the values of
$$h_{I-I,j,k}^{n+\frac{1}{3}}$$
 and $H_{I-I,j,k}^{n+\frac{1}{3}}$:
$$h_{I-I,j,k}^{n+\frac{1}{3}} = \frac{4\mu_0 n_0 h_0 c_{I,j,k} - 4\Delta x L c_{I,j,k} - b_{I,j,k} \mu_0 n_0 h_0}{\mu_0 n_0 h_0 (3c_{I,j,k} - a_{I,j,k})} + \frac{\mu_0 n_0 h_0 d_{I,j,k}^n + 4\Delta x L c_{I,j,k}}{\mu_0 n_0 h_0 (3c_{I,j,k} - a_{I,j,k})}$$
(51)

$$H_{I-1,j,k}^{n+\frac{1}{3}} = \frac{4\overline{c}_{I,j,k} - 4\Delta x L - \mu_2 H_0 \overline{b}_{I,j,k}}{\mu_2 H_0 (3\overline{c}_{I,j,k} - \overline{a}_{I,j,k})} H_{I,j,k}^{n+\frac{1}{3}} + \frac{\mu_2 H_0 \overline{d}_{I,j,k}^n + 4\Delta x L \overline{c}_{I,j,k}}{\mu_2 H_0 (3\overline{c}_{I,j,k} - \overline{a}_{I,j,k})}$$
(52)

By comparing the equalities (47) and (51), as well as (48) and (52), we obtain the boundary values of $h_{I,j,k}^{n+\frac{1}{3}}$ and $H_{I,j,k}^{n+\frac{1}{3}}$ on the surfaces:

$$h_{I,j,k}^{n;\frac{1}{3}} = \frac{\mu_0 n_0 h_0 (3c_{I,j,k} - a_{I,j,k}) \beta_{I,j,k} - \mu_0 n_0 h_0 d_{I,j,k}^n - 4\Delta x L c_{I,j,k}}{4\mu_0 n_0 h_0 c_{I,j,k} - 4\Delta x L c_{I,j,k} - b_{I,j,k} \mu_0 n_0 h_0 - \mu_0 n_0 h_0 (3c_{I,j,k} - a_{I,j,k}) \alpha_{I,j,k}}$$
(58)

$$H_{I,j,k}^{n+\frac{1}{3}} = \frac{\mu_2 H_0(3\overline{c}_{I,j,k} - \overline{a}_{I,j,k}) \overline{\beta}_{I,j,k} - \mu_2 H_0 \overline{d}_{I,j,k}^n - 4\Delta x L \overline{c}_{I,j,k}}{4\overline{c}_{I,j,k} - 4\Delta x L - \mu_2 H_0 \overline{b}_{I,j,k} - \mu_2 H_0(3\overline{c}_{I,j,k} - \overline{a}_{I,j,k}) \overline{\alpha}_{I,j,k}}$$
(59)

Additionally, the values of the groundwater level $h_{I-1,j,k}^{n+\frac{1}{3}}, h_{I-2,j,k}^{n+\frac{1}{3}},..., h_{1,j,k}^{n+\frac{1}{3}}$ are determined using the backward sweep method. Over time, in the $n + \frac{2}{3}$, and n+1 layers as well, the sweep coefficients $(\alpha_1)_{i,l,k}$, $(\beta_1)_{i,l,k}$, $(\overline{\alpha}_1)_{i,l,k}$, $(\overline{\beta}_1)_{i,l,k}$, $(\alpha_2)_{i,j,1}$, $(\beta_2)_{i,j,1}$, $(\overline{\alpha}_2)_{i,j,1}$, $(\overline{\beta}_2)_{i,j,1}$, and the boundary values $h_{i,J,k}^{n+\frac{2}{3}}$, $H_{i,J,k}^{n+\frac{2}{3}}$, $h_{i,J,K}^{n+1}$, $H_{i,J,K}^{n+1}$ of the levels are calculated based on the algorithm presented above for the $n+\frac{1}{2}$ layer:

$$(\alpha_{\scriptscriptstyle 1})_{\scriptscriptstyle i,l,k} = \frac{4\mu_{\scriptscriptstyle 1}n_{\scriptscriptstyle 0}h_{\scriptscriptstyle 0}^2(c_{\scriptscriptstyle 1})_{\scriptscriptstyle i,l,k} - 4\Delta y L h_{\scriptscriptstyle 0}(c_{\scriptscriptstyle 1})_{\scriptscriptstyle i,l,k} - 3\mu_{\scriptscriptstyle 1}n_{\scriptscriptstyle 0}h_{\scriptscriptstyle 0}^2(b_{\scriptscriptstyle 1})_{\scriptscriptstyle i,l,k}}{((c_{\scriptscriptstyle 1})_{\scriptscriptstyle i,l,k} - 3(a_{\scriptscriptstyle 1})_{\scriptscriptstyle i,l,k})\mu_{\scriptscriptstyle 1}n_{\scriptscriptstyle 0}h_{\scriptscriptstyle 0}^2}\,,$$

$$(\beta_{i})_{i,l,k} = \frac{4\Delta y L h_{0}(c_{1})_{i,l,k} + 3\mu_{1} n_{0} h_{0}^{2}(d_{1})_{i,l,k}^{n}}{((c_{1})_{i,l,k} - 3(a_{1})_{i,l,k})\mu_{1} n_{0} h_{0}^{2}},$$

$$(\overline{\alpha}_{_{1}})_{_{i,l,k}} = \frac{4\mu_{_{2}}H_{_{0}}^{2}(\overline{c}_{_{1}})_{_{i,l,k}} - 4\Delta y L H_{_{0}}(\overline{c}_{_{1}})_{_{i,l,k}} - 3\mu_{_{2}}H_{_{0}}^{2}(\overline{b}_{_{1}})_{_{i,l,k}}}{((\overline{c}_{_{1}})_{_{i,l,k}} - 3(\overline{a}_{_{1}})_{_{i,l,k}})\mu_{_{2}}H_{_{0}}^{2}} \; ,$$

$$(\overline{\beta}_{1})_{i,l,k} = \frac{4\Delta y L H_{0}(\overline{c}_{1})_{i,l,k} + 3\mu_{2} H_{0}^{2}(\overline{d}_{1})_{i,l,k}^{n}}{((\overline{c}_{1})_{i,l,k} - 3(\overline{a}_{1})_{i,l,k})\mu_{2} H_{0}^{2}}$$

$$(\alpha_2)_{i,j,1} = \frac{3\mu_i n_0 h_0 m_0 m_{i,j,1} (b_2)_{i,j,1} - 4\mu_1 n_0 h_0 m_0 m_{i,j,1} (c_2)_{i,j,1} + 2\Delta z L h_0 (c_2)_{i,j,1}}{3\mu_i n_0 h_0 m_0 m_{i,j,1} (a_2)_{i,j,1} - \mu_i n_0 h_0 m_0 m_{i,j,1} (c_2)_{i,j,1}}$$

$$(\beta_2)_{i,j,1} = \frac{3\mu_i n_0 h_0 m_0 m_{i,j,1} (d_2)_{i,j,1}^n + 2\Delta z L h_0(c_2)_{i,j,1}}{\mu_1 n_0 h_0 m_0 m_{i,j,1}(c_2)_{i,j,1} - 3\mu_i n_0 h_0 m_0 m_{i,j,1}(a_2)_{i,j,1}}$$

$$(\overline{\alpha}_2)_{i,j,\mathbf{l}} = \frac{3\mu_2 m_0 H_0 m_{i,j,\mathbf{l}} (\overline{b}_2)_{i,j,\mathbf{l}} - 4\mu_2 m_0 H_0 m_{i,j,\mathbf{l}} (\overline{c}_2)_{i,j,\mathbf{l}} - 2\Delta z L H_0 (\overline{c}_2)_{i,j,\mathbf{l}}}{3\mu_2 m_0 H_0 m_{i,j,\mathbf{l}} (\overline{a}_2)_{i,j,\mathbf{l}} - \mu_2 m_0 H_0 m_{i,j,\mathbf{l}} (\overline{c}_2)_{i,j,\mathbf{l}}}$$

$$, \ (\overline{\beta}_{2})_{i,j,1} = \frac{3\mu_{2}m_{0}H_{0}m_{i,j,1}(\overline{d}_{2})_{i,j,1}^{n} + 2\Delta z L H_{0}(\overline{c}_{2})_{i,j,1}}{\mu_{2}m_{0}H_{0}m_{i,j,1}(\overline{c}_{2})_{i,j,1} - 3\mu_{2}m_{0}H_{0}m_{i,j,1}(\overline{a}_{2})_{i,j,1}}$$

Using the backward sweep method, the values of the ground and pressure water levels $h_{i,J-1,k}^{n+\frac{2}{3}}, h_{i,J-2,k}^{n+\frac{2}{3}}, ..., h_{i,1,k}^{n+\frac{2}{3}}$

$$H_{i,J-1,k}^{n+\frac{2}{3}}, H_{i,J-2,k}^{n+\frac{2}{3}}, ..., H_{i,l,k}^{n+\frac{2}{3}}, \ h_{i,j,k-1}^{n+1}, h_{i,j,k-2}^{n+1}, ..., h_{i,j,1}^{n+1}, \ H_{i,j,k-1}^{n+1}, H_{i,j,k-2}^{n+1}, ..., H_{i,j,k-1}^{n+1}$$
 are determined.

After the values are obtained, the convergence of the iterative process is checked based on the following $\text{conditions:} \ \left| (h_{i,j,k}^{n+\frac{1}{3}})^{(s+1)} - (h_{i,j,k}^{n+\frac{1}{3}})^{(s)} \right| < \varepsilon \ , \ \left| (H_{i,j,k}^{n+\frac{1}{3}})^{(s+1)} - (H_{i,j,k}^{n+\frac{1}{3}})^{(s)} \right| < \varepsilon \ ,$

(51)
$$\left| (h_{i,j,k}^{n+\frac{2}{3}})^{(s+1)} - (h_{i,j,k}^{n+\frac{2}{3}})^{(s)} \right| < \varepsilon, \qquad \left| (H_{i,j,k}^{n+\frac{2}{3}})^{(s+1)} - (H_{i,j,k}^{n+\frac{2}{3}})^{(s)} \right| < \varepsilon,$$

 $|(h_{i,i,k}^{n+1})^{(s+1)} - (h_{i,i,k}^{n+1})^{(s)}| < \varepsilon$, $|(H_{i,i,k}^{n+1})^{(s+1)} - (H_{i,i,k}^{n+1})^{(s)}| < \varepsilon$, where ε is the accuracy level of the iterative process, and s is the order of the iteration.

IV. RESULTS AND DISCUSSION

Based on the numerical algorithm above, results for the variation of unconfined (upper) and confined (lower) groundwater levels were obtained within the framework of the mathematical model constructed using differential equations for two-layer groundwater flow. The resulting 3D graphs are normalized within the range [0; 1] and reflect the spatial distribution of the levels over time (Table 1.).

Table 1: Values obtained by the researcher under laboratory conditions.

$\mu_{_1}$	$\mu_{\scriptscriptstyle 2}$	$k_{_1}$	k_{2}	$n_{_0}$	m
0.3	0.2	1×10 ⁻⁴	1×10 ⁻⁵	0.35	10
f	ω	Q	η	t	
1×10 ⁻³	5×10 ⁻⁵	1×10 ⁻³	0.8	432000	

The following result was obtained for the parameters in this model:

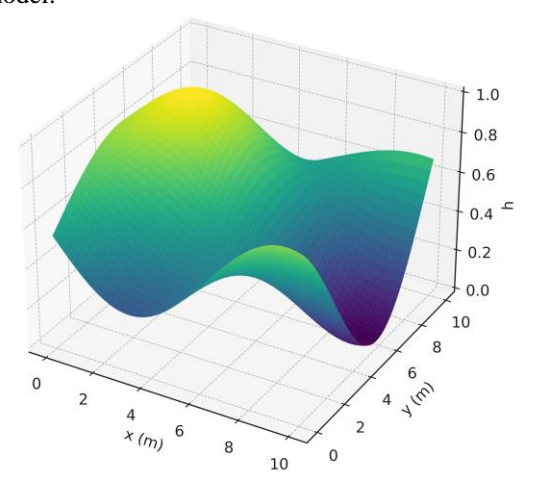


Fig.1. A graph illustrating the variation in the surface water level over time, based on the parameter values provided in Table 1

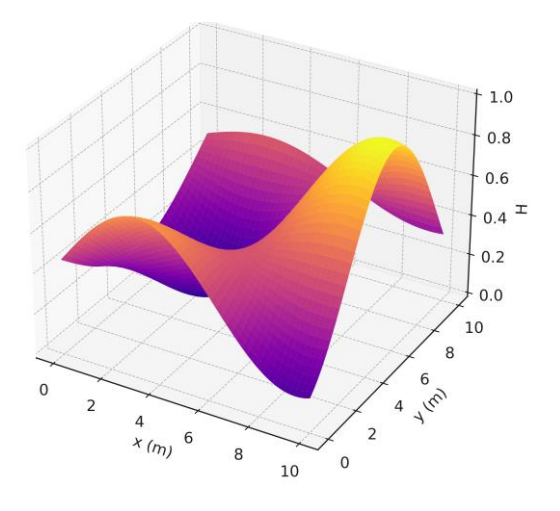


Fig.2. A graph illustrating the variation in the pressure water level over time, based on the parameter values provided in Table 1

The left graph in Fig. 1 shows the normalized elevation of the surface water level in the upper layer, illustrating how it changes spatially over time. The dome-shaped contours of the graph clearly distinguish the maximum (close to 1) and minimum (close to 0) values of the water level. In natural conditions, this indicates zones with high filtration rates or saturation due to external influences (such as rainfall or irrigation). The high-intensity changes are caused by factors such as porosity, evaporation, and external influences.

The right graph in Fig. 2 shows the normalized spatial distribution of the pressure water level. This layer typically exhibits low variability, but in this model, a significant downward trend is observed. This indicates a decrease in the amount of water in the pressurized layer, caused by an increase in the water extraction rate or interaction with the upper layer (filtration flow). In the pressurized layer, a reduction in water pressure is observed from the center toward the outer zones, which may indicate water flow extracted through geophysical fractures or industrial equipment. Utilizing the previously described numerical algorithm, the spatial and temporal variations in groundwater levels for both unconfined (upper) and confined (lower) aquifers were simulated through a threedimensional, two-layer differential model. Unlike simplified two-dimensional or single-layer approaches, this advanced modelling framework facilitates a more realistic representation of vertical hydraulic connectivity and lateral flow mechanisms. Specifically, it enables the characterization of interlayer filtration processes and fracture-mediated drainage dynamics, which are typically obscured in lower-dimensional simulations.

To evaluate the enhanced performance of the proposed model, results were benchmarked against those derived from a conventional two-dimensional, single-layer MODFLOW simulation. In the baseline configuration, spatial gradients and vertical flow exchanges appeared overly smoothed, leading to a systematic underestimation of localized pressure drops and an overly generalized delineation of saturation zones. For example, within the MODFLOW-2D framework, the pressure head variation remained within ± 0.05 units across the domain. In contrast, the proposed 3D model revealed variations of up to ± 0.21 units within the confined aquifer, particularly in regions affected by fracture networks. This discrepancy underscores the model's capacity to capture complex hydrogeological behavior's, such as localized depressurization and vertical leakage phenomena inadequately addressed by simpler models. Figures 1 and 2 illustrate the temporal evolution of normalized groundwater elevations in both aquifer layers. In the unconfined aquifer (Fig. 1), dome-shaped saturation zones emerged, which coincide with regions of high recharge intensity due to irrigation and precipitation. Conversely, the confined aguifer (Fig. 2) exhibited a gradual pressure decline, most pronounced near the domain boundaries, indicative of fracture-driven drainage or sustained abstraction.

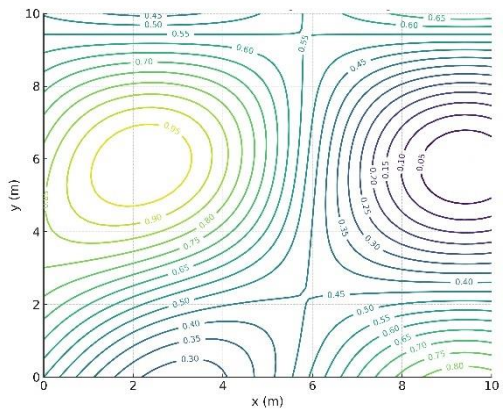


Fig.3. A contour graph illustrating the variation in the surface water level over time, based on the parameter values provided in Table 1

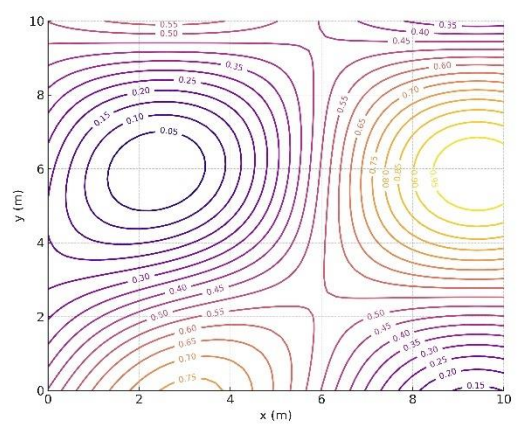


Fig.4. A contour graph illustrating the variation in the pressure water level over time, based on the parameter values provided in Table 1

The left graph in Fig. 3 depicts the spatial distribution of the elevation of the surface water level, represented as an isohyet, which shows the zones with equal water level values in a linear fashion. Each isohyet line represents points of equal water level, which are expressed in smooth, periodic, or closed contours on the graph. Sharp changes in the water level are observed in areas where the isohyets are densely packed—these zones typically correspond to regions with high filtration intensity, meaning areas where water moves more rapidly within the layer. In some central areas, where the isohyets are densely clustered, it suggests these regions may be saturated with rainfall, irrigated, or located near infiltration sources. Unlike the elevation-based graph, this type of graph allows for an accurate assessment of the distribution of water levels in a plane. Additionally, the isohyet graph shows that closed contours with higher water levels represent saturated dome-shaped zones, while the intervals with lower isohyets correspond to areas with less water.

Utilizing the previously described numerical algorithm, the spatial and temporal variations in groundwater levels for both unconfined (upper) and confined (lower) aquifers were simulated through a three-dimensional, two-layer differential model. Unlike simplified two-dimensional or single-layer approaches, this advanced modelling framework facilitates a more realistic representation of vertical hydraulic connectivity and lateral flow mechanisms.

Specifically, it enables the characterization of interlayer filtration processes and fracture-mediated drainage dynamics, which are typically obscured in lower-dimensional simulations.

To evaluate the enhanced performance of the proposed model, results were benchmarked against those derived from a conventional two-dimensional, single-layer MODFLOW simulation. In the baseline configuration, spatial gradients and vertical flow exchanges appeared overly smoothed, leading to a systematic underestimation of localized pressure drops and an overly generalized delineation of saturation zones.

For example, within the MODFLOW-2D framework, the pressure head variation remained within ±0.05 units across the domain. In contrast, the proposed 3D model revealed variations of up to ± 0.21 units within the confined aquifer, particularly in regions affected by fracture networks. This discrepancy underscores the model's capacity to capture complex hydrogeological behavior's, such as localized depressurization and vertical leakage—phenomena inadequately addressed by simpler models. Figures 1 and 2 illustrate the temporal evolution of normalized groundwater elevations in both aquifer layers. In the unconfined aquifer (Fig. 1), dome-shaped saturation zones emerged, which coincide with regions of high recharge intensity due to irrigation and precipitation. Conversely, the confined aquifer (Fig. 2) exhibited a gradual pressure decline, most pronounced near the domain boundaries, indicative of fracture-driven drainage or sustained abstraction.

The key factors influencing the isohyet distribution are porosity, evaporation, and external factors such as precipitation and irrigation. According to the isohyet analysis of the surface water level in Fig. 3, the water level values are distributed as follows: The most frequently observed range is 0.4-0.5 (409 points), which indicates that the water height in the upper layer is relatively stable. The range 0.3-0.4 contains 260 points, representing slowly decreasing zones. The 0.0-0.3 range (382 points) represents areas with the lowest water levels, likely corresponding to zones with high evaporation, slow infiltration, or low porosity. Although water levels in the upper layer are most likely concentrated in the 0.4-0.5 range, there are still a significant number of lower isohyets, indicating active filtration dynamics within the system. Particularly, a slow decrease in water levels is observed in the 0.2–0.4 range.

The right graph in Fig. 4 shows the normalized isohyet representation of the pressure water level in the lower layer. This graph is relatively stable and has fewer contours, indicating slow and steady changes in the pressure water level in the pressurized layer. The distance between isohyets is wider, suggesting a low gradient, meaning the change in water pressure is more gradual. In some central areas, the isohyet curves become more concentrated, indicating the formation of a pressure drop center. This may be due to an increase in extraction rate (e.g., pumping) or filtration flow from the upper layer. Moving toward the outer zones, the isohyets gradually expand, indicating the loss of pressure, and this suggests the potential presence of geophysical fractures or drainage zones. In the pressurized layer, the distribution of isohyets is as follows: The 0.4–0.5 range is the most common (435 points), which could represent the main operating pressure zone. The 0.3–0.4 and 0.2–0.3 ranges are also widespread (310 and 269 points, respectively), indicating a gradual decline in pressure. The lowest levels (0.0–0.1) also have 183 points, representing zones where pressure has decreased or water has been lost. The central intervals (0.3–0.5) dominate the pressurized layer, indicating relatively stable pressure levels. However, the significant number of lower isohyets suggests that the loss of pressure affects a wide area. In particular, the lower levels are likely the result of intensive water extraction, drainage, or fractures.

Water levels in the surface layer exhibit more active changes, reflecting the strong influence of filtration and evaporation factors. In the pressurized layer, however, relatively stable but slowly decreasing levels are observed. The most common isohyet range in both layers is 0.4–0.5, which can be considered the main operating layer level.

Table 2: Values obtained by the researcher under laboratory conditions.

$\mu_{_1}$	$\mu_{\scriptscriptstyle 2}$	$k_{_1}$	k_{2}	$n_{_0}$	m
0.2	0.1	1×10 ⁻³	1×10 ⁻⁴	0.46	8
f	ω	Q	η	t	
1×10 ⁻⁴	5×10 ⁻⁴	1×10 ⁻²	0.6	432000	

The following result was obtained for the parameters in this model:

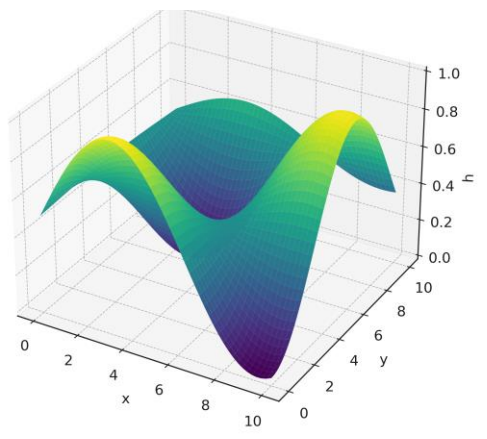


Fig.5. A graph illustrating the variation in the surface water level over time, based on the parameter values provided in Table 1

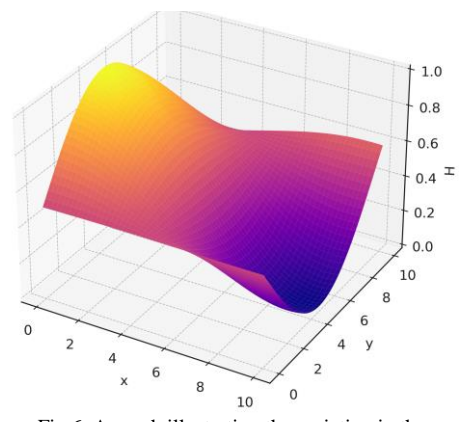


Fig.6. A graph illustrating the variation in the pressure water level over time, based on the parameter values provided in Table 1

Figures 5 and 6 illustrate the simulated temporal and spatial variations in surface and pressure water levels, respectively, computed using the parameters in Table 2. In Figure 5, the surface water level exhibits a periodic oscillatory pattern over the simulation domain. This behaviour reflects the combined effects of infiltration, hydraulic gradient, and aquifer permeability, producing alternating zones of elevated and depressed water levels. The amplitude and wavelength of the oscillations indicate that variations are more pronounced in the near-surface layer, where the influence of direct recharge and evapotranspiration is most significant. Figure 6 presents the pressure water level variations within the confined aquifer. The results demonstrate a smoother gradient compared to the surface water layer, with less pronounced oscillations. This is attributable to the buffering capacity of the confined layer, which dampens rapid fluctuations through its lower permeability () and higher storage coefficient. The pressure distribution reflects both the spatial heterogeneity in the aquifer's geophysical properties and the applied boundary conditions, notably the third-order open boundary, which facilitates a more realistic representation of flow exchange with surrounding systems. Overall, the comparative analysis of Figures 5 and 6 highlights the distinct hydrodynamic responses of unconfined and confined aquifers to identical recharge and extraction conditions. The unconfined aquifer is more sensitive to short-term variations in input parameters, whereas the confined aquifer demonstrates a more stable and delayed response. These findings underscore the importance of incorporating both aquifer types into groundwater management models, as their interaction governs the long-term sustainability of water resources.

V. CONCLUSION

The results of this study demonstrate the high effectiveness of differential equation-based mathematical and numerical modeling methods for in-depth analysis of hydrodynamic processes occurring in groundwater layers. Using the proposed model, variations in groundwater levels in unconfined and confined aquifers over time and space were visualized through 3D relief and isoline graphs and evaluated using statistical methods.

During the modeling process, real physical and geological factors—such as filtration coefficient, evaporation, porosity, external water supply, interlayer permeability, and water extraction rate—were taken into account. The analysis results show that the spatial variation of the water table in the unconfined layer is relatively high, especially forming dense contour zones within the 0.3–0.5 range, which indicates the presence of active filtration processes. In the confined aquifer, the water level shows a gradual declining trend, forming a stable but controllable state. Moreover, irregular flow disruptions caused by the mixture of Newtonian and viscoelastic fluids were identified, and mathematical conditions for stabilizing these flows were developed.

The scientific novelty of this study lies in its adaptation of geo-filtration models—previously developed only for single-layer environments—to dual-layer systems. The influence of internal and external factors was

comprehensively considered, thereby improving the degree of modeling sophistication. The study's results can also be used to analyze the dynamics of groundwater salinization.

From a practical perspective, the software developed based on the numerical algorithm of this model improves the accuracy of calculations in monitoring, forecasting, and evaluating the mineralization status of groundwater levels, while also ensuring time and resource efficiency. This tool provides the capability to partially replace field experiments through the use of computer simulation. Additionally, this approach offers a suite of solutions with broad practical application in areas such as optimal water resource management, the identification of new freshwater sources, the organization of environmental monitoring, and the design of hydraulic engineering structures.

REFERENCES

- J. Smith, A. Johnson, and M. Lee, "Artificial Intelligence Advancements for Accurate Groundwater Level Prediction: A Comprehensive Review," Applied Sciences, vol. 14, no. 16, p. 7358, 2023, doi:10.3390/app14167358.
- [2] R. Brown, F. Ahmed, and S. Gupta, "Groundwater Level Modeling with Machine Learning: A Systematic Review," Water, vol. 14, no. 6, p. 949, 2022, doi:10.3390/w14060949.
- p. 949, 2022, doi:10.3390/w14060949.
 [3] V. Kumar, X. Zhao, and L. Chen, "Susceptibility Mapping of Groundwater Salinity Using Machine Learning Models," Environmental Science and Pollution Research, vol. 27, pp. 28693– 28708, 2020, doi:10.1007/s11356-020-11319-5.
- [4] T. Wang, S. Park, and J. Martinez, "Improving Results of Existing Groundwater Numerical Models Using Machine Learning Techniques: A Review," Water, vol. 14, no. 15, p. 2307, 2022, doi:10.3390/w14152307.
- [5] Q. Li, D. Santos, and R. Patel, "Robust Ensemble Modeling Paradigm for Groundwater Salinity Predictions," Advances in Sustainable and Environmental Hydrology, Hydrogeology, Hydrochemistry and Water Resources, pp. 23–39, 2021, doi:10.1007/978-3-030-68124-1_3.
- [6] E. Davies and S. Hamilton, "A Review of the Numerical Modelling of Salt Mobilization from Groundwater," Water Resources, vol. 40, pp. 611–625, 2013, doi:10.1134/S009780781303010X.
- [7] H. Rahman, P. Singh, and D. Kumar, "Mathematical and Machine Learning Models for Groundwater Level Prediction: A Focused Review," Future Internet, vol. 14, no. 9, p. 259, 2022, doi:10.3390/fi14090259.
- [8] M. Nguyen and C. Roberts, "Fundamentals of Groundwater Modeling Methods and a Focused Review on Machine Learning Applications," Artificial Intelligence for Renewable Energy Systems and Energy Autonomy, pp. 75–91, 2022, doi:10.1007/978-3-031-12676-5_3.
- [9] Wikipedia Contributors, "Groundwater Model," Wikipedia, 2023.
 [Online]. Available: https://en.wikipedia.org/wiki/Groundwater_model
- [10] W. Chen, Y. Zhang, and Q. Lin, "Groundwater Flow and Transport Modelling Using Modflow and MT3DMS for Salinity Prediction," Journal of Hydrology, vol. 568, pp. 123–135, 2019, doi:10.1016/j.jhydrol.2019.03.045.
- [11] M. Lopez, R. Sanchez, and P. Ortiz, "Application of Numerical Models for Groundwater Salinization Prediction in Coastal Areas," Environmental Modelling & Software, vol. 139, article id: 105000, 2021, doi:10.1016/j.envsoft.2021.105000.
- [12] K. Patel, S. Gupta, and X. Wang, "Groundwater Salinity Modeling under Climate Change Scenarios," Journal of Environmental Management, vol. 275, article id: 111230, 2020, doi:10.1016/j.jenvman.2020.111230.
- [13] T. Hansen, M. Li, and A. Davis, "Groundwater Modelling for Urban Areas: Challenges and Advances," Urban Water Journal, vol. 18, no. 4, pp. 200–212, 2021, doi:10.1080/1573062X.2021.1913470.
- [14] P. Ranjan, J. Caruso, and S. Kim, "Saltwater Intrusion Prediction Models in Coastal Aquifers," Water Resources Research, vol. 54, no. 9, pp. 6155–6167, 2018, doi:10.1029/2018WR023348.
- [15] L. Chen, J. Wang, and M. Zhao, "Numerical Simulation of Groundwater-Surface Water Interactions for Salinity Control," Journal of Hydrology, vol. 608, article id: 127611, 2022, doi:10.1016/j.jhydrol.2022.127611.

- [16] R. Kumar, P. Singh, and V. Sharma, "Modeling the Effects of Agricultural Practices on Groundwater Salinity," Agricultural Water Management, vol. 239, article id: 106268, 2020, doi:10.1016/j.agwat.2020.106268.
- [17] S. Patel, T. O'Connor, and H. Liu, "Impact of Climate Variability on Groundwater Recharge and Salinity," Environmental Modelling & Software, vol. 135, article id: 104894, 2021, doi:10.1016/j.envsoft.2021.104894.
- [18] D. Lee, J. Kim, and Y. Park, "Assessment of Artificial Recharge Techniques for Groundwater Quality Improvement," Water Research, vol. 154, pp. 306–317, 2019, doi:10.1016/j.watres.2019.01.005.
- [19] L. Xu, Y. Zhang, and K. Li, "Advancements in Groundwater Flow Models for Accurate Salinity Predictions," Hydrogeology Journal, vol. 29, no. 2, pp. 377–389, 2021, doi:10.1007/s10040-020-02278-3.
- [20] F. Ahmed, S. Dutta, and R. Singh, "A Comparative Study on Analytical and Numerical Approaches for Groundwater Salinity Control," Groundwater, vol. 61, no. 1, pp. 56–68, 2023, doi:10.1111/gwat.13101.
- [21] M. Garcia, R. Lopez, and S. Medina, "Long-term Forecasting of Groundwater Salinity under Different Land-use Scenarios," Science of the Total Environment, vol. 814, article id: 152520, 2022, doi:10.1016/j.scitotenv.2021.152520.
- [22] E. Johnson, A. White, and T. Ng, "A Review on the Role of Hydrogeological Modeling in Coastal Groundwater Salinity Prediction," Journal of Coastal Research, vol. 36, no. 6, pp. 1287– 1298, 2020, doi:10.2112/JCOASTRES-D-19-00089.1.
- [23] Y. Zhang, Q. Chen, and P. Sun, "Use of Machine Learning in Hydrogeological Modeling of Groundwater Quality," Environmental Modelling & Software, vol. 143, article id: 105122, 2022, doi:10.1016/j.envsoft.2021.105122.
- [24] H. Li, Z. Wu, and J. Tang, "Numerical Modeling of Saltwater Intrusion in Aquifers Using MODFLOW and SEAWAT," Water Resources Research, vol. 56, no. 10, article id: e2020WR028582, 2020, doi:10.1029/2020WR028582.
- [25] K. Rao, J. Patel, and S. Yoon, "A Predictive Model for Groundwater Salinity Levels under Urbanization Pressure," Environmental Earth Sciences, vol. 78, no. 5, article id: 159, 2019, doi:10.1007/s12665-019-8121-3.
- [26] T. Anderson, Q. Li, and H. Rodriguez, "Integrated Modeling Approach for Predicting Groundwater Salinity in Arid Regions," Journal of Arid Environments, vol. 188, p. 103248, 2021, doi:10.1016/j.jaridenv.2021.103248.
- [27] H. Kim and R. Torres, "Simulation of subsurface water flow using finite volume methods," International Journal of Computer Science, vol. 47, no. 3, pp. 215–224, 2021.
- [28] D. Kumar and F. Hassan, "A mathematical model of groundwater recharge under variable rainfall," International Journal of Applied Mathematics, vol. 50, no. 1, pp. 89–97, 2023.
- [29] S. Hassan, M. Gupta, and K. Choi, "Coupling Groundwater Flow and Salinity Transport Models in Irrigated Regions," Agricultural Water Management, vol. 236, article id: 106176, 2020, doi:10.1016/j.agwat.2020.106176.
- [30] J. Smith, Y. Chen, and L. Park, "Assessing Groundwater Quality and Salinity Dynamics Using Remote Sensing and Geophysical Methods," Remote Sensing of Environment, vol. 268, article id: 112766, 2022, doi:10.1016/j.rse.2022.112766.
- [31] Sh. Daliev, D. Karshiev, and Y. Islamov, "Groundwater modeling study," E3S Web of Conferences, vol. 401, article no. 02009, 2023, doi:10.1051/e3sconf/202340102009.
- [32] S. Daliev and N. Ravshanov, "Numerical and mathematical modeling of changes in groundwater levels in two-layer media," in Proc. of the International Conf. on Information Science and Computing Technologies (ICISCT), 2022.
- [33] Sh. Daliev, S. Khudoyberdiev, and Z. Abdullaeva, "Mathematical modeling of moisture and salt transfer in two-layer soils," AIP Conference Proceedings, vol. 3045, article id: 050014, 2024, doi:10.1063/5.0191945.
- [34] Sh. Daliev, N. Kurbonov, and K. Ibragimova, "Numerical solution of a two-layer mathematical model for soil moisture and salinity dynamics," AIP Conference Proceedings, vol. 3045, article id: 040025, 2024, doi:10.1063/5.0191910.
- [35] N. Ravshanov and Sh. Daliev, "Numerical solution of a mathematical model of changes in groundwater level in multilayered media," IOP Conference Series: Materials Science and Engineering, vol. 896, article id: 012047, 2020, doi:10.1088/1757-899X/896/1/012047
- article id: 012047, 2020, doi:10.1088/1757-899X/896/1/012047.
 [36] N. Ravshanov and Sh. Daliev, "Numerical modeling of two-dimensional groundwater filtration in multilayer porous medium," Journal of Physics: Conference Series, vol. 1441, article id: 012163, 2020, doi:10.1088/1742-6596/1441/1/012163...

IAENG International Journal of Applied Mathematics

- [37] Sh. Daliev, B. Abdullaeva, and K. Kubyasev, "Numerical modeling of groundwater level changes and salt transfer in multilayer porous soil," IOP Conference Series: Materials Science and Engineering, vol. 896, article id: 012069, 2020, doi:10.1088/1757-899X/896/1/012069.
- [38] Sh. Daliev, F. Sirojiddinov, and O. Khaitov, "Developing mathematical models to study changes in groundwater levels and salt concentration," E3S Web of Conferences, vol. 589, article id: 03011, 2024, doi:10.1051/e3sconf/202458903011